Inorganica Chimica Acta 565 (2024) 122005

Contents lists available at ScienceDirect

Inorganica Chimica Acta

journal homepage: www.elsevier.com/locate/ica

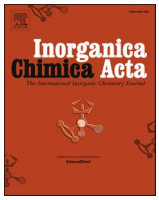

Activity of (η^6-arene)dichloridoruthenium(II) complexes with antifungal imidazolyl-based ligands against *Toxoplasma gondii* and *Leishmania major*

Ibrahim S. Al Nasr [a], Ismail Daoud [b,c], Waleed S. Koko [d], Tariq A. Khan [e], Rainer Schobert [f], Ridha Ben Said [g,h], Noureddine Amdouni [h], Seyfeddine Rahali [g], Ali O. Al-Ghamdi [i], Bernhard Biersack [f,*]

[a] Department of Biology, College of Science, Qassim University, Qassim 51452, Saudi Arabia
[b] Department of Matter Sciences, University Mohamed Khider, BP 145 RP, Biskra 07000, Algeria
[c] Laboratory of Natural and Bio-active Substances, Faculty of Science, Tlemcen University, P.O. Box 119, Tlemcen 13000, Algeria
[d] Department of Science Laboratories, College of Science and Arts, Qassim University, Ar Rass 51921, Saudi Arabia
[e] Department of Clinical Nutrition, College of Applied Health Sciences, Qassim University, Ar Rass 51921, Saudi Arabia
[f] Organic Chemistry Laboratory, University Bayreuth, Universitätsstrasse 30, 95440 Bayreuth, Germany
[g] Department of Chemistry, College of Science and Arts, Qassim University, Ar Rass 51921, Saudi Arabia
[h] Laboratoire de Caractérisations, Applications et Modélisations des Matériaux, Faculté des Sciences de Tunis, Université Tunis El Manar, Tunis, Tunisia
[i] Biology Department, Faculty of Science and Arts, El Mekhwah, Al-Baha University, Al-Baha, Saudi Arabia

ARTICLE INFO

Keywords:
Ruthenium
Azoles
Clotrimazole
Bifonazole
*Tg*CDPK1
Neglected tropical diseases

ABSTRACT

A series of six (η^6-arene)Ru(II) complexes with antifungal imidazole drug ligands such as clotrimazole, bifonazole and climbazole was prepared and analyzed. They were tested for their activities against *Leishmania major* and *Toxoplasma gondii* parasites, and were compared with the activities of the metal-free azole ligands. Activities superior to those of the azole ligands were observed for the Ru complexes, which indicate the beneficial role of the (η^6-arene)ruthenium(II) moiety in terms of antiparasitic properties. The modifications of the arene ligand also played a role in the biological activity. Docking of selected ruthenium complexes into *T. gondii* kinase CDPK1 and ADME-T calculations revealed promising binding affinities and drug-like properties.

1. Introduction

Metal salts and complexes are salient drugs for the treatment of various human ailments. Platinum(II) complexes are highly active against cancer, silver ions are prominent antibiotics, vanadium compounds can treat diabetes, and gold complexes alleviate rheumatoid arthritis [1]. Various drugs made of the metalloids arsenic and antimony (e.g., melarsoprol, glucantime and pentostam) are used for the treatment of protozoal parasite infections such as leishmaniasis and sleeping sickness (i.e., human African trypasonomiasis/HAT), while the boron-based drug acoziborole is currently in clinical trials for advanced HAT [2]. In line with platinum complexes, other platinum-group metal complexes such as ruthenium complexes were described as attractive anticancer drug candidates, and the "iconic" Ru(III) complexes NAMI-A and KP1019 underwent clinical trials [3,4]. In terms of piano-stool (arene)Ru(II) complexes, noteworthy drug candidates are anti-metastatic complexes with pta (1,3,5-triaza-7-phosphaadamantane) ligands (i.e., RAPTA complexes), as well as various cytotoxic $[(arene)Ru(en)Cl]^+$ complexes, which were able to overcome cisplatin-resistance in cancer cells [5–8]. The identification of anticancer active (arene)Ru(II) *N*-heterocyclic carbene (NHC) complexes is another remarkable development [9,10]. More recently, (*p*-cymene)Ru(II) NHC complexes with 1,3-dialkylbenzimidazol-2-ylidene ligands exhibited antileishmanial activity [11]. Several Ru(II) and Ru(III) complexes were described as antiviral, antibacterial, antifungal, and antiparasitic drug candidates [12]. The tremendous scope of organometallic platinum-group metal complexes as antimalarial agents was recently summarized, too [13]. In terms of antiparasitic ruthenium complexes, pioneering work was done by the group of Sánchez-Delgado, who likewise resolved the potential of ruthenium complexes with widely applied azole-based antifungals [14,15]. Several complexes of clotrimazole and other azoles with metals such as platinum, gold, copper, zinc, cobalt, and nickel and their antiparasitic, anticancer, and antimicrobial activities were described. Since iron binding of target cytochromes is essential for azole drugs, these

* Corresponding author.
E-mail address: bernhard.biersack@yahoo.com (B. Biersack).

https://doi.org/10.1016/j.ica.2024.122005
Received 3 January 2024; Received in revised form 17 February 2024; Accepted 4 March 2024
Available online 5 March 2024

metal-based azole compounds likely act by different mechanisms of action, which might contribute to increased biological activities and the circumvention of azole-related resistance mechanisms [16–18].

As immune-compromised people are at risk of severe complications when infected with the globally occurring *Toxoplasma gondii* parasites (i.e., the causative agents of toxoplasmosis), new drugs for the treatment of toxoplasmosis in such patients are necessary [19]. Leishmaniasis is categorized as a neglected tropical disease (NTD) and clinically subdivided into visceral leishmaniasis (VL), cutaneous leishmaniasis (CL), and mucocutaneous leishmaniasis (MCL). The CL form brought about by various *Leishmania* species such as *L. major*, *L. tropica*, *L. mexicana*, *L. amazonensis* etc., causes severe skin lesions. It is the most prevalent leishmaniasis form responsible for up to 1 million, mostly young, patients annually [20,21]. Although usually not lethal, CL leads to stark and disfiguring skin lesions and to stigmatization of affected persons [22,23]. CL patients are currently treated with pentavalent antimonials, miltefosine, amphotericin or pentamidine [21]. Aside of the general toxicity of clinically applied drugs such as antimonials, another growing problem is the emergence of drug-resistant parasite forms. Thus, new potent anti-parasitic drugs against leishmaniasis are needed.

Since the first report of an antifungal azole, benzimidazole, in 1944, and the approval of chlormidazole for clinical application in 1958, the class of azole fungicides has expanded to a valuable and still growing arsenal of drugs predominantly used for the treatment of systemic and superficial mycoses [24,25]. In line with the described antiparasitic preclinical data on antifungal azole metal complexes, the antiparasitic potential of approved azole fungicides was frequently studied and documented, since CYP51 targeting/inhibition appears to exert antiparasitic activities, too [26,27]. Clotrimazole and bifonazole showed activity against *L. infantum chagasi* promastigotes, however, clotrimazole was inactive against *T. gondii* [28,29]. To our knowledge, no antiparasitic activities have been reported for climbazole, yet. While clotrimazole and bifonazole are antifungal drugs applied and approved for human and veterinary health care, climbazole is an over-the-counter fungicidal component of personal care products such as anti-dandruff shampoos and dermal cosmetics [30].

In the present report, a series of new η^6-benzene and η^6-*p*-cymene ruthenium complexes with antifungal imidazole ligands (clotrimazole, bifonazole and climbazole, Fig. 1) was prepared and tested for activity against *L. major* and *T. gondii* parasites. The obtained antiparasitic results were compared with activities of the azole ligands and with a known antiparasitic ruthenium complex analog.

2. Results and discussion

2.1. Chemistry

The (arene)Ru(II) complexes **1a–f** were prepared from the reaction of one equivalent $[RuCl_2(\eta^6\text{-arene})]_2$ with two equivalents imidazole (clotrimazole/CTZ, bifonazole/BFZ or climbazole/CBZ, Scheme 1) [12]. Only **1b** was published before as a potent antileishmanial, and, thus, it was included into this study as a positive control (η^6-arene)Ru(II) complex [14]. The complexes were obtained as powdered brown (η^6-benzenes **1a**, **1c**, and **1e**) or amber solids (η^6-*p*-cymenes **1b**, **1d**, and **1f**) in moderate yields. They showed high solubility in organic solvents and solvent mixtures including acetone, ethyl acetate, and chlorinated solvents (CH_2Cl_2, $CHCl_3$). ^1H and ^{13}C NMR spectra of the complexes recorded in $CDCl_3$ indicate successful complex formation, and displayed the azole ligand signals together with the corresponding η^6-arene (*p*-cymene or benzene) signals. As expected, the η^6-arene protons were shifted to higher fields in the ^1H NMR spectra (multiplets between 5.5 and 5.7 ppm for the η^6-benzene complexes, and doublets of coupling constants of 6.0–6.1 Hz between 5.1 and 5.5 ppm for the η^6-*p*-cymene complexes), when compared with ordinary arene proton signals. In terms of ESI HR-MS data, the target complexes (dissolved in acetonitrile and MS run in H_2O/acetonitrile mixtures) were found without one of

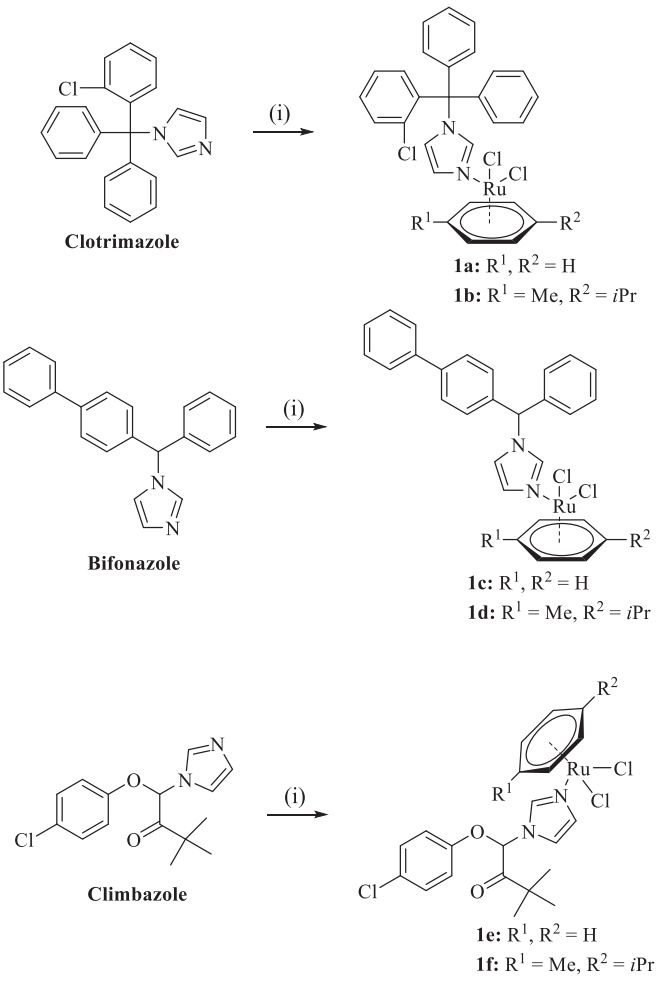

Scheme 1. Reagents and conditions: (i) $[Ru(benzene)Cl_2]_2$, acetone, 70 °C, 3 h for **1a**, **1c**, **1e**; $[Ru(p\text{-cymene})Cl_2]_2$, CH_2Cl_2, r.t., 3 h for **1b**, **1d**, **1f**; 43–68 %.

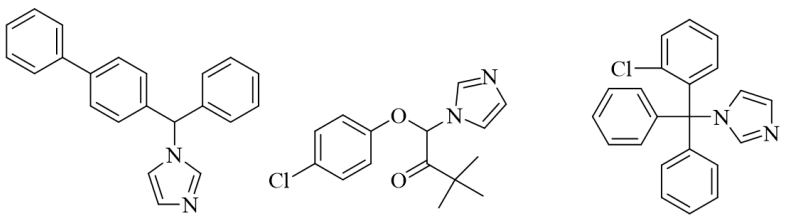

Fig. 1. Structures of the antifungal azole drugs bifonazole, climbazole, and clotrimazole.

their chlorido ligands, which matches with mass spectrometric data of dichlorido(η^6-arene)Ru(II) complexes from pertinent literature (Figures S1-S5, Supporting Information) [31]. These mass spectrometry findings are a hint at a labile chlorido ligand in the complexes and a preferred mono-substitution/hydrolysis of the complexes in line with the hydrolysis pattern of previously described dichlorido(η^6-arene)Ru(II) complexes such as RAPTA-C [32].

2.2. Antiparasitic activity

The ruthenium complexes **1a–f** were initially tested for their activity against *T. gondii* tachyzoites (Table 1). The approved antiparasitic drug atovaquone was applied as a positive control [33]. Complex **1d** was the most active compound against *T. gondii*, closely followed by **1b**, **1a**, and **1e**. In addition, this is the first report on anti-*Toxoplasma* activity by the known complex **1b**. *T. gondii* cells were also more sensitive to these complexes than Vero cells, and **1e** showed the highest selectivity index (SI = 9.3) of all tested complexes. Only **1c** showed a greater toxicity to Vero cells than to *T. gondii*. The metal-free azole ligands clotrimazole and climbazole were distinctly less active than their metal complexes **1a**/**1b** and **1e**/**1f**, which is in line with previous reports of clotrimazole inactivity against *T. gondii* [29]. In contrast to that, bifonazole showed considerable anti-*Toxoplasma* activity with relatively low toxicity to Vero cells, albeit complex **1d** was more active, and complex **1e** more active and selective than bifonazole. Notably, **1e** and bifonazole were much less toxic to Vero cells than the approved antiparasitic drugs atovaquone and amphotericin B. Bifonazole is a dual CYP51/HMG-CoA inhibitor in contrast to clotrimazole and climbazole, which might explain its higher activity against *T. gondii* in comparison to the activity of the other two tested azoles [34].

The activity of complexes **1a–f** against *L. major* promastigotes and amastigotes was also determined (Table 2). The approved anti-leishmanial drug amphotericin B was applied as positive control [33]. Complex **1d** showed the highest activity against promastigotes, closely followed by **1b**, **1a**, and **1f**. Clotrimazole, bifonazole and climbazole, and the complexes **1c** and **1e** were inactive against *L. major* parasites. The inactivity of **1e** is remarkable since it was active against *T. gondii* parasites. Notably, complex **1a** was the only η^6-benzene complex with considerable activity against *L. major* promastigotes, and the *p*-cymene ligand appears to be superior to the benzene ligand in *L. major*. The observed antileishmanial activity was largely independent of the respective azole ligand. *L. major* amastigotes were slightly less sensitive to the complexes than the promastigotes. Complex **1b** was the most active compound against the amastigotes, closely followed by **1f** and **1d**. η^6-Benzene complex **1a** was less active against amastigotes than its close η^6-*p*-cymene congener **1b**. Among the active Ru complexes, **1a** and **1f** were less toxic to macrophages than amphotericin B. The toxicity of complexes **1b** and **1d** was comparable with the toxicity of amphotericin B.

Table 1
Inhibitory concentrations IC_{50} (in μM) of complexes **1a–f** and their metal-free azole ligands clotrimazole, bifonazole and climbazole when applied to cells of the Vero (African green monkey kidney epithelial) cell line, and when applied to cells of *Toxoplasma gondii*.[a] Amphotericin B (AmB, Vero) and atovaquone (ATO, Vero and *T. gondii*) were applied as positive controls for the indicated cells.

Compd.	IC_{50} (*T. gondii*)	IC_{50} (Vero)	SI (Vero / *T. gondii*)[b]
1a	2.6 ± 0.3	8.5 ± 1.7	3.3
1b	2.5 ± 0.3	6.5 ± 1.1	2.6
1c	8.7 ± 1.4	3.8 ± 0.6	0.4
1d	2.1 ± 0.2	7.6 ± 0.9	3.6
1e	3.9 ± 0.5	36.4 ± 5.2	9.3
1f	10.4 ± 2.1	16.2 ± 2.8	1.6
Clotrimazole	14.6 ± 2.6	22.7 ± 3.4	1.6
Bifonazole	5.8 ± 0.7	42.2 ± 6.5	7.3
Climbazole	>45.1	>45.1	–
AmB[c]	–	7.7 ± 1.2	–
ATO[c]	0.07 ± 0.02	9.5 ± 1.5	136

[a] Values are the means of at least three independent experiments (±SD). They were obtained from concentration–response curves by calculating the percentage of treated cells in comparison to untreated controls after 72 h. [b]Selectivity index (SI) was calculated from the corresponding IC_{50} values for the Vero cells and *T. gondii*. [c]Values were taken from ref. [33].

Table 2
Inhibitory concentrations IC_{50} (in μM) of complexes **1a–f** and their metal-free azole ligands clotrimazole, bifonazole and climbazole when applied to promastigotes and amastigotes of *Leishmania major* and macrophages.[a] Amphotericin B (AmB) was applied as a positive control.

Compd.	IC_{50} promastigotes	IC_{50} amastigotes	Macrophages
1a	6.9 ± 0.8	15.8 ± 2.4	14.7 ± 2.2
1b	5.7 ± 0.9	9.4 ± 1.6	7.5 ± 1.3
1c	>35.7	–	25.5 ± 3.9
1d	5.2 ± 0.6	11.8 ± 2.1	9.1 ± 1.5
1e	>36.8	–	>36.8
1f	8.5 ± 1.3	10.5 ± 1.7	15.4 ± 2.8
Clotrimazole	39.1 ± 4.7	>39.4	39.1 ± 5.4
Bifonazole	>42.5	>42.5	41.6 ± 6.6
Climbazole	>45.1	>45.1	41.3 ± 4.7
AmB[b]	0.8 ± 0.2	0.5 ± 0.1	8.1 ± 0.1

[a] Values are the means of three experiments (±SD). They were obtained from concentration–response curves by calculating the percentage of treated cells in comparison to untreated controls after 72 h. [b]Values were taken from ref [33].

Although the previously reported antileishmanial activity of **1b** seemed to be more impressive than its activity determined in this work, our study confirmed the antileishmanial potential of **1b**, and of the new complexes **1a**, **1d**, and **1f** [14]. Discrepancies in activities reported by different research groups might be explained by differences in assays and assay conditions, as well as by the condition of the applied parasite strain. Notably, complex **1b** (also dubbed AM160), and even more its acetylacetonate (acac) chelate complex analog AM162, were active in a murine model of cutaneous leishmaniasis, and were tolerated well by the treated mice [35]. Thus, the investigation of in vivo activities of complexes **1a–f** in suitable *T. gondii* models can be taken into account for future studies. The SI value (Vero/*T. gondii*) of the new complex **1e** is nearly 10, which is a recommended selectivity for the identification of new hit compounds against protozoal parasites [36]. This was corroborated by studies with the drug clindamycin, which is clinically applied for the treatment of *T. gondii* infections and displayed an SI value of 10.9 [37]. The anti-toxoplasmal drug atovaquone, which was used in this study, has some drawbacks such as resistance induction and prophylaxis/treatment failure, which necessitates the development of new drugs against *T. gondii* [38]. Moreover, the combination of atovaquone with other drugs has the potential to overcome resistance mechanisms. For example, atovaquone/proguanil was developed as a combination therapy against *Plasmodium falciparum*, after early clinical studies had shown that atovaquone as a single agent was associated with recurrence of highly atovaquone-resistant infections in a considerable number of patients [39]. Future studies will show if the most promising Ru complexes described in this work will have the potential to replace, or synergize with, atovaquone in the treatment of apicomplexan parasites.

2.3. TgCDPK1 docking and drug-likeness calculations

In order to carry out docking calculations, optimized structures of complexes **1d** and **1e** and atovaquone were made (Fig. 2). The complexes exhibited a *pseudo*-tetrahedral geometry with the azole, *p*-cymene, Cl1, and Cl2 ligands. In complex **1d** the Ru–C_i (i = 1 to 6) bond lengths were 2.242 Å, 2.239 Å, 2.257 Å, 2.275 Å, 2.242 Å and 2.255 Å, respectively. The Ru–N, Ru–Cl1, and Ru–Cl2 bond distances were 2.099 Å, 2.448 Å, and 2.503 Å, respectively, which are in line with literature values [40]. The geometry of the **1d** complex is a distorted tetrahedron based on the steric hindrance of the η^6-interaction of *p*-cymene. Therefore, the average *N*-Ru-C_i, Cl1-Ru-C_i and Cl2-Ru-C_i bond angles were

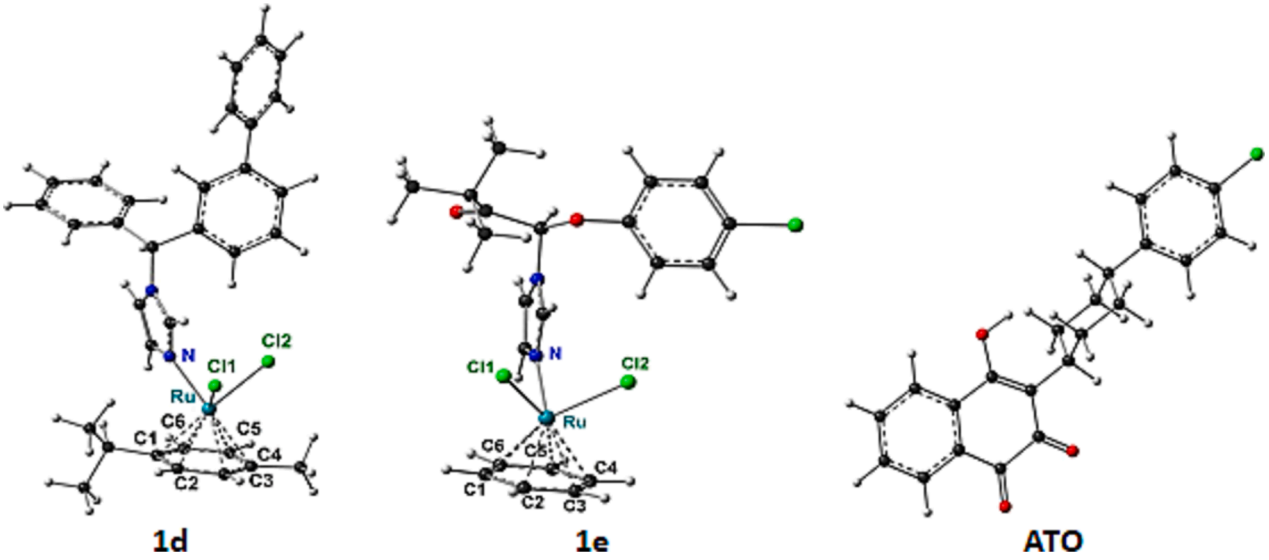

Fig. 2. Optimized geometry of the most active compounds **1d**, **1e**, and ATO.

125.2°, 120.4° and 120.2°, respectively, and all these angles were greater than 109°. The same observations were found for complex **1e**. The selected bond lengths and angles for the complexes **1d** and **1e** are summarized in Table 3.

Using molecular docking in computer-aided drug discovery and design has become essential to investigate interactions with possible protein targets [41,42]. The computer-generated three-dimensional structure of possible ligands is positioned into a receptor structure using molecular docking in various orientations and conformations. Within this framework, we conducted docking simulations using **1d**, **1e**, and the standard medication ATO to the specific binding site of *T. gondii* calcium-dependent protein kinase 1 (*Tg*CDPK1, PDB ID: 4JBV). *Tg*CDPK1 is a CaM (calmodulin/calcium kinase) family serine-threonine kinase of *T. gondii*, which connects calcium signaling with parasite pathogenicity [43]. It provides the opportunity to develop selective *Tg*CDPK1-targeting drugs (in particular, bumped kinase inhibitors/BKIs) with low side-effects because of the expanded ATP-binding pocket of *Tg*CDPK1 with a glycine gate-keeper residue [44,45]. *N*-heterocyclic BKIs such as BKI-1748 revealed pronounced antitoxoplasmal activity in infected mice and sheep [46,47]. Since ruthenation of azoles likely abrogates CYP51 interaction, we investigated *Tg*CDPK1 as a possible target instead.

Table 3
Selected bond lengths (Å) and angles (°) for complexes **1d** and **1e**.

Complex	1d	1e
Ru-N	2.099	2.085
Ru-Cl1	2.448	2.443
Ru-Cl2	2.503	2.451
Ru-C1	2.242	2.254
Ru-C2	2.239	2.258
Ru-C3	2.257	2.258
Ru-C4	2.275	2.263
Ru-C5	2.242	2.252
Ru-C6	2.255	2.263
Cl1-Ru-N	87.8	85.7
Cl2-Ru-N	82.4	85.0
C1-Ru-N	95.3	95.9
C2-Ru-N	119.7	119.4
C3-Ru-N	156.6	156.0
C4-Ru-N	159.6	160.0
C5-Ru-N	122.6	123.0
C6-Ru-N	97.5	97.5
Cl1-Ru-C1	118.9	118.6
Cl1-Ru-C2	90.9	91.1
Cl1-Ru-C3	88.3	89.3
Cl1-Ru-C4	112.1	114.0
Cl1-Ru-C5	149.3	151.2
Cl1-Ru-C6	155.9	155.6
Cl2-Ru-C1	149.8	151.6
Cl2-Ru-C2	157.8	155.6
Cl2-Ru-C3	120.8	118.5
Cl2-Ru-C4	92.3	91.4
Cl2-Ru-C5	88.9	89.4
Cl2-Ru-C6	112.8	144.5

The best *Tg*CDPK1 docking poses of compounds **1d**, **1e** and ATO are shown in Table 4. The standard parameters of the BIOVIA DS visualization package (Dassault Systèmes BIOVIA, Discovery Studio modeling environment, 2020) were used to visualize interactions between the compounds and the target. The test candidates demonstrated their ability to bind to the active site of the target by several types of interactions, justified by low docking score (S-score) values. Molecular docking results confirmed that **1d** and **1e** have high affinities for the pocket site of *Tg*DPK1, which is confirmed by the highest negative score values (-161.876 and −132.808 kcal/mol, respectively) compared with ATO (-83.651 kcal/mol, Table 4). Complex **1d** established two strong hydrogen bonds with residues LEU57 and LYS59 (bonds distance = 2.64 and 2.82 Å, respectively) (Table 4, Fig. 3) [48]. In addition, **1d** formed two electrostatic interactions (π-cation) with ARG442 and nine hydrophobic interactions with VAL65, LEU57, LEU345, ALA342, LYS338, and ALA446. Complex **1e** formed four strong hydrogen bonds with LYS80, GLY60, and LEU57 (at bonds distances = 2.18, 1.57, 3.06, and 2.95 Å) [48]. Moreover, **1e** exhibited twelve hydrophobic interactions with LEU57, ILE194, LEU181, LYS80, MET112, and VAL65 (Table 4, Fig. 3). Notably, the η^6-arene rings contributed to the binding of the complexes to the *Tg*CDPK1 binding site. Molecular docking analysis revealed certain similarities in the binding of *Tg*CDPK1 by **1d** and ATO, which can be attributed to the mutual interaction with four crucial *Tg*CDPK1 residues (LYS59, ARG442, LYS338, and LEU345). Interactions with these residues were also described for triazole-modified ursolic acid-based *Tg*CDPK1 inhibitors [49]. To our knowledge, no metal-based *Tg*CDPK1 inhibitors are known, and more in vitro studies are required to elucidate the interaction of ruthenium complexes with *Tg*CDPK1.

Drug-likeness screening predicts the likelihood that a molecule possesses desired drug-like qualities and physical features, which are referred to as drug-like attributes. It is possible to describe drug-like qualities as intrinsic properties of a molecule, which are essential in the drug discovery process [50–52]. The SwissADME server (https://www.swissadme.ch/) was used to calculate important drug-likeness parameters and physicochemical properties (Table 5) [53]. The

Table 4
Docking results of the compounds **1d**, **1e**, and standard drug ATO with the binding site of calcium-dependent protein kinase-1 *Tg*CDPK1 (pdb 4jbv).

Compounds	MolDock Score (kcal/mol)	Bonds between atoms of compounds and active site residues					
		Atom of compound	Involved receptor atoms	Involved receptor residues	Category	Type	Distance (Å)
1d	−161.876	H2	O	LEU57	H-Bond	Carbonyl H-Bond	2.64
		/	NH	LYS59	H-Bond	π-Donor H-Bond	2.82
		/	NH1	ARG442	Electrostatic	π-Cation	4.54
		/	NH1	ARG442	Electrostatic	π-Cation	3.25
		Cl1	/	VAL65	Hydrophobic	Alkyl	4.35
		C29	/	LEU57	Hydrophobic	Alkyl	4.32
		C29	/	VAL65	Hydrophobic	Alkyl	4.54
		/	/	LEU57	Hydrophobic	π-Alkyl	5.29
		/	/	LEU345	Hydrophobic	π-Alkyl	4.86
		/	/	ALA342	Hydrophobic	π-Alkyl	5.44
		/	/	LYS338	Hydrophobic	π-Alkyl	4. 88
		/	/	ALA342	Hydrophobic	π-Alkyl	4.99
		/	/	ALA446	Hydrophobic	π-Alkyl	3.96
1e	−132.808	O1	HZ1	LYS80	H-Bond	Conventional H-Bond	2.18
		O1	HA1	GLY60	H-Bond	Carbonyl H-Bond	1.57
		O1	HE2	LYS80	H-Bond	Carbonyl H-Bond	3.06
		H4	O	LEU57	H-Bond	Carbonyl H-Bond	2.95
		Cl1	/	LEU57	Hydrophobic	Alkyl	3.97
		Cl2	/	LEU57	Hydrophobic	Alkyl	3.47
		C13	/	ILE194	Hydrophobic	Alkyl	4.92
		C15	/	LEU181	Hydrophobic	Alkyl	4.55
		C15	/	ILE194	Hydrophobic	Alkyl	3.97
		Cl3	/	LYS80	Hydrophobic	Alkyl	4.40
		Cl3	/	MET112	Hydrophobic	Alkyl	4. 37
		/	/	LEU181	Hydrophobic	π-Alkyl	5.22
		/	/	VAL65	Hydrophobic	π-Alkyl	4.40
		/	/	LYS80	Hydrophobic	π-Alkyl	4.52
		/	/	MET112	Hydrophobic	π-Alkyl	5.45
		/	/	ILE194	Hydrophobic	π-Alkyl	4.40
ATO	−83.651	/	NH	LYS59	H-Bond	π-Donor H-Bond	3.21
		/	NH1	ARG442	Electrostatic	π-Cation	4.38
		/	NH1	ARG442	Electrostatic	π-Cation	4.90
		/	OE1	GLU178	Electrostatic	π-Cation	3.90
		/	/	LYS338	Hydrophobic	Amide-π Stacked	4.59
		Cl1	/	PHE333	Hydrophobic	π-Alkyl	5.12
		/	/	LYS338	Hydrophobic	π-Alkyl	4.71
		/	/	LEU345	Hydrophobic	π-Alkyl	5.10

number of hydrogen bond donors for compounds **1d** and **1e** is <**7** (*n*-HD: 0 ∼ 7) and the number of hydrogen bond acceptors is <12 (*n*-HA: 0 ∼ 12). We also note that the molecular weight value of **1d** does not fall into the interval of 100 ∼ 600 g/mol, while **1e** does. In addition, all MLogP, WLogP values of these compounds were >5 except for the MLogP value of compound **1e**. Besides, the nROTB numbers of complexes **1d** and **1e** were <11. Overall, these findings suggest that **1d** adheres to the Veber rule but does not meet the criteria of Lipinski and Egan rules due to several violations of the molecular weight and LogP values. On the other hand, complex **1e** obeys the Lipinski and Veber rules but does not comply with the Egan rule. Furthermore, the TPSA values of **1d** and **1e** are both less than 140 Å. This indicates that both compounds have good permeability in the cytoplasmic membrane and blood–brain barrier (BBB), which are important drug transport parameters. Evidently, this discovery indicates favorable oral bioavailability and pharmacokinetic properties of both ruthenium complexes. However, it is possible that differences may occur between the described in silico data and future in vivo pharmacological findings for these complexes.

Fig. 4 illustrates the optimal area for each bioavailable attribute, represented by the pink-colored section. The following parameters were included: molecular weight (SIZE), lipophilicity (LIPO), polarity (POLAR), insolubility (INSOLU), insaturation (INSATU), and flexibility (FLEX). The examined complexes **1d** and **1e** were located inside the colored zone and within FLEX, POLOR, and INSATU categories. Furthermore, both compounds possessed a comparable average molecular weight and insolubility. The compounds were outside the boundary of the LIPO-colored zone.

3. Conclusions

Promising results were obtained from the evaluation of a small series of ruthenium complexes as potential drugs against pathogenic parasites such as *T. gondii* and *L. major*, which can cause severe infections in humans. Some of the tested (η^6-arene)Ru(II) complexes were especially active against *T. gondii* parasites, which appears to be a relevant target pathogen for ruthenium-based therapeutics. The higher sensitivity of apicomplexan *T. gondii* for the described ruthenium complexes when compared with *L. major* kinetoplastid parasites was remarkable and might be applicable for the identification of further sensitive protozoal pathogens. For instance, other apicomplexan parasites such as *Plasmodium* species, the causative agents of malaria disease, might also be sensitive to ruthenium treatment. In addition, feasible combinations of the most active (arene)Ru(II) complexes with approved anti-parasitic drugs can be useful in order to optimize their efficacy, and to reduce the minimal effective dosage and possible side-effects in future animal studies.

Complexes **1d** and **1e** underwent molecular docking simulations and ADME-T predictions. Both compounds displayed high affinities for the target pocket of *Tg*CDPK1 as to low MolDock score values and the formation of multiple interactions with the target site. Moreover,

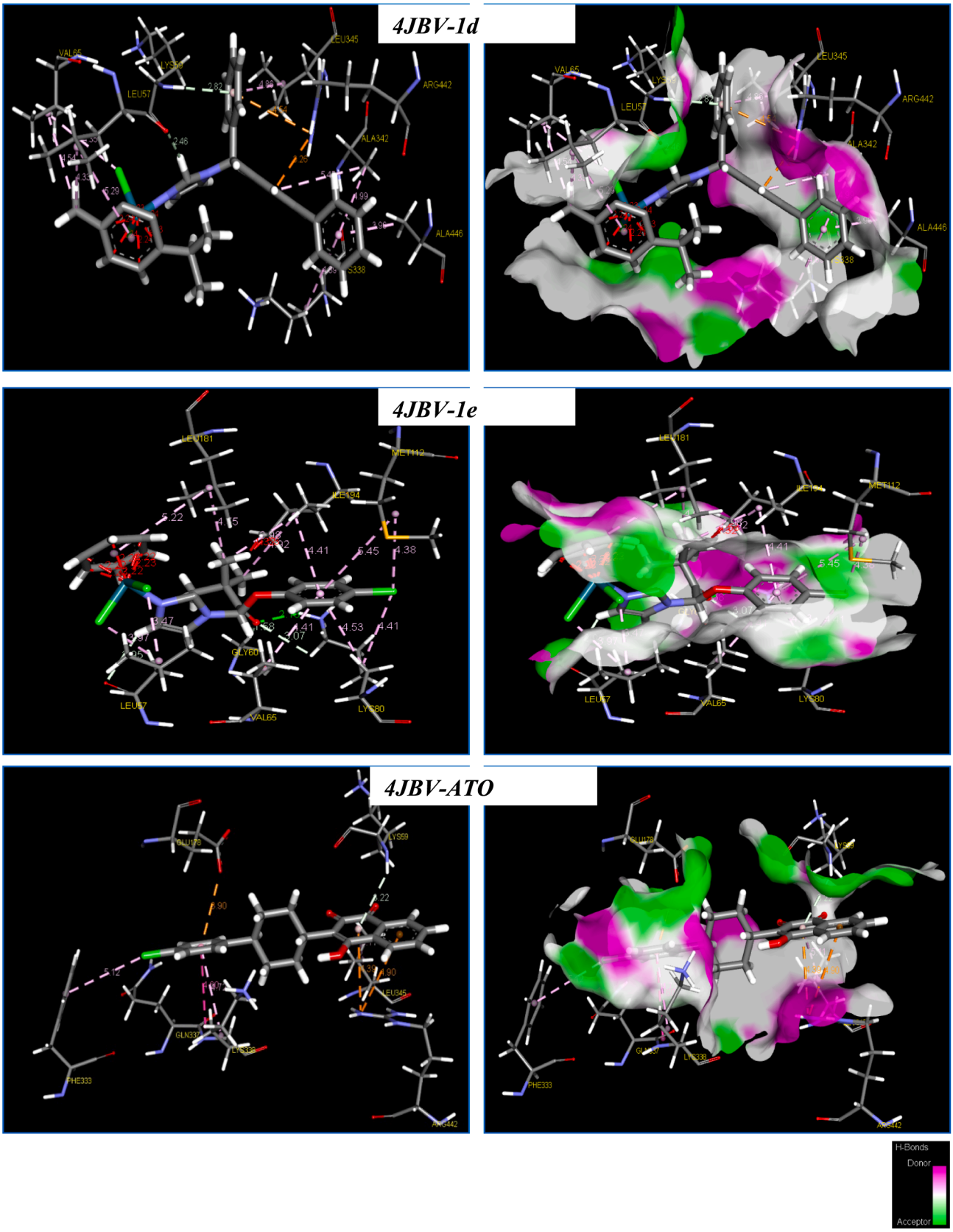

Fig. 3. 3D diagram of interactions of the compounds **1d**, **1e**, and ATO with the active site residues of *Tg*CDPK1 (pdb: 4JBV).

Table 5
Physicochemical properties and drug likeliness of compounds **1d** and **1e**.

Compounds	Physicochemical property						Drug likeliness		
	TPSA ($Å^2$)	*n*-ROT	MW (g/mol)	MLog P / WLogP	*n*-HA	*n*-HD	Lipinski	Veber	Egan
	(0 ~ 140)	(0 ~ 11)	(100 ~ 600)	(0 ~ 5)	(0 ~ 12)	(0 ~ 7)			
1d	9.86	6	616.59	6.27 10.01	0	0	Rejected	Accepted	Rejected
1e	36.16	6	555.87	3.50 6.94	2	0	Accepted	Accepted	Rejected

TPSA: Topological Polar Surface Area**, *n*-ROT:** Number of Rotatable, **MW:** Molecular Weight**, Log P:** Logarithm of partition coefficient of compound between *n*-octanol and water**, *n*-HA:** Number of hydrogen bond acceptors**, *n*-HD:** Number of hydrogen bonds donors.

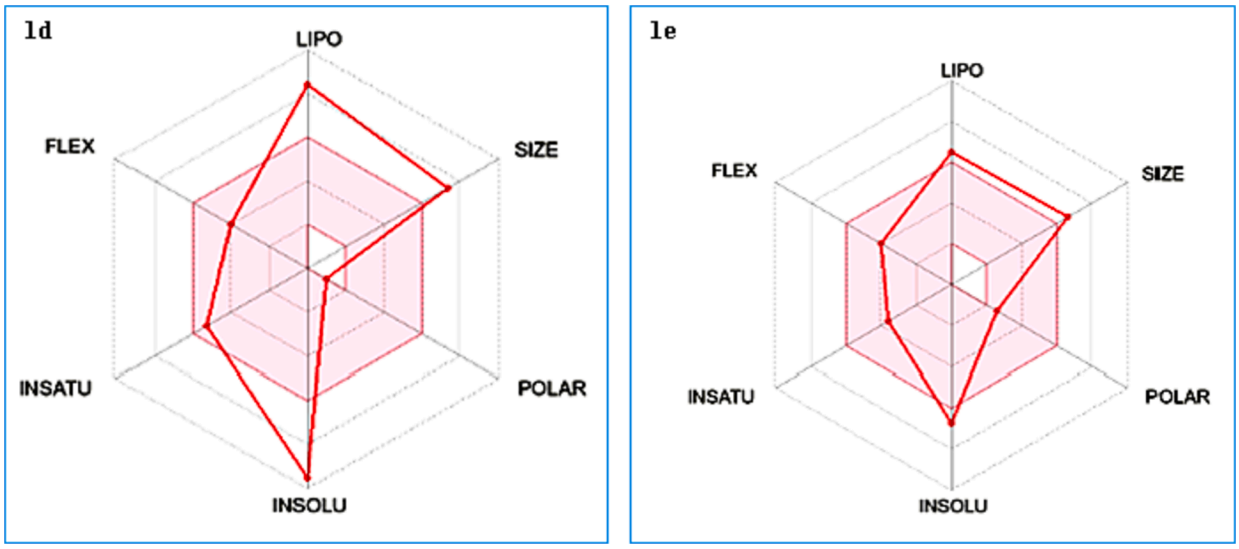

Fig. 4. Bioavailability radar of compounds **1d** and **1e** using SwissADME software [50].

physicochemical properties of these complexes demonstrated a high level of drug-likeness. The molecular docking and ADME predictions underlined the potential of **1d** and **1e** as promising antitoxoplasmal drug candidates, which need to be confirmed by future in vitro and in vivo experiments.

4. Experimental

4.1. Chemistry

Complex **1b** was prepared following a literature procedure, and analyzed. The obtained analytical data correlated with published data of this complex [12]. Synthetic procedures and analytical data of the new complexes are given below. All starting compounds and solvents were purchased from the usual chemical vendors and used without further purification. Melting points (uncorrected), Electrothermal 9100; NMR spectra, Bruker Avance 300 spectrometer; chemical shifts are given in parts per million (δ) downfield from tetramethylsilane as internal standard; IR, Perkin-Elmer Spectrum One FT-IR spectrophotometer equipped with an ATR sampling unit; ESI and high-resolution mass spectra were measured with a UPLC/Orbitrap (ESI-HRMS); Elemental analyses, Perkin-Elmer 2400 CHN elemental analyzer.

4.1.1. Dichlorido(benzene)(CTZ)ruthenium(II) ***(1a)***

Clotrimazole (39 mg, 0.114 mmol) was dissolved in acetone (5 mL) and $[Ru(benzene)Cl_2]_2$ (29 mg, 0.057 mmol) was added. The reaction mixture was stirred at 70 °C for 3 h. *n*-Hexane (50 mL) was added and the formed precipitate was collected, washed with *n*-hexane and dried in vacuum. Yield: 46 mg (0.077 mmol, 68 %); brown solid of m.p. > 200 °C (dec.); ^{1}H NMR (300 MHz, $CDCl_3$): δ 5.5–5.6 (6H, m), 6.76 (1H, s), 6.9–7.0 (1H, m), 7.1–7.2 (4H, m), 7.3–7.4 (9H, m), 7.4–7.5 (1H, m), 7.93 (1H, s); ^{13}C NMR (75 MHz, $CDCl_3$): δ 84.0 (η^6-benzene-CH), 121.7 (imidazole-CH), 128.3, 128.5, 129.9, 130.4, 131.0, 131.3 (Ar-CH), 132.2 (imidazole-CH), 135.4 (Ar-C_q), 139.4 (Ar-C_q), 139.8 (imidazole-CH), 142.4 (Ar-C_q); HRMS for $C_{28}H_{23}N_2Cl_2Ru$ [M^+ - Cl] calcd. 559.02763, found 559.02865; Anal. Calc. for $C_{28}H_{23}N_2Cl_3Ru$: C, 56.53; H, 3.90; N, 4.71; found: C, 56.48; H, 3.93; N, 4.75.

4.1.2. Dichlorido(*p*-cymene)(CTZ)ruthenium(II) (1b) [10]

Clotrimazole (39 mg, 0.114 mmol) was dissolved in CH_2Cl_2 (5 mL) and $[Ru(p\text{-cymene})Cl_2]_2$ (35 mg, 0.057 mmol) was added. The reaction mixture was stirred at room temperature for 3 h. *n*-Hexane (50 mL) was added and the formed precipitate was collected, washed with *n*-hexane and dried in vacuum. Yield: 43 mg (0.066 mmol, 58 %); amber solid; ^{1}H NMR (300 MHz, $CDCl_3$): δ 1.17 (6H, d, J = 6.9 Hz), 2.07 (3H, s), 2.9–2.9 (1H, m), 5.10 (2H, d, J = 6.0 Hz), 5.29 (2H, d, J = 6.0 Hz), 6.79 (1H, s), 6.9–7.0 (1H, m), 7.1–7.2 (4H, m), 7.2–7.4 (9H, m), 7.4–7.5 (1H, m), 7.82 (1H, s).

4.1.3. Dichlorido(benzene)(BFZ)ruthenium(II) ***(1c)***

Bifonazole (35 mg, 0.114 mmol) was dissolved in acetone (5 mL) and $[Ru(benzene)Cl_2]_2$ (29 mg, 0.057 mmol) was added. The reaction mixture was stirred at 70 °C for 3 h. *n*-Hexane (50 mL) was added and the formed precipitate was collected, washed with *n*-hexane and dried in vacuum. Yield: 36 mg (0.064 mmol, 56 %); brown solid of mp > 200 °C (dec.); ^{1}H NMR (300 MHz, $CDCl_3$): δ 5.6–5.7 (6H, m), 6.51 (1H, s), 6.79

(1H, m), 7.0–7.2 (3H, m), 7.3–7.5 (9H, m), 7.5–7.6 (3H, m), 7.97 (1H, s); ^{13}C NMR (75 MHz, $CDCl_3$): δ 65.9 (*N*-CH), 84.0 (η^6-benzene-CH), 119.5 (imidazole-CH), 127.1, 127.7, 128.0, 128.5, 128.9, 129.1 (Ar-CH), 132.2 (imidazole-CH), 137.8 (Ar-C_q), 136.7 (Ar-C_q), 139.8 (imidazole-CH), 140.8 (Ar-C_q), 142.2 (Ar-C_q); HRMS for $C_{28}H_{24}N_2ClRu$ [M^+ - Cl] calcd. 525.06660, found 525.06745; Anal. Calc. for $C_{28}H_{24}N_2Cl_2Ru$: C, 60.00; H, 4.32; N, 5.00; found: C, 60.12; H, 4.27; N, 4.97.

4.1.4. Dichlorido(p-cymene)(BFZ)ruthenium(II) **(1d)**

Bifonazole (35 mg, 0.114 mmol) was dissolved in CH_2Cl_2 (5 mL) and [Ru(*p*-cymene)Cl_2]$_2$ (35 mg, 0.057 mmol) was added. The reaction mixture was stirred at room temperature for 3 h. Ethyl acetate / *n*-hexane (1:4, 50 mL) was added and the formed precipitate was collected, washed with *n*-hexane and dried in vacuum. Yield: 48 mg (0.078 mmol, 68 %); amber solid of mp > 110 °C (dec.); ν_{max} (ATR)/cm^{-1}: 3113, 3057, 3030, 2961, 2921, 2868, 1601, 1487, 1470, 1452, 1410, 1387, 1323, 1226, 1199, 1157, 1107, 1086, 1057, 1030, 1007, 859, 822, 803, 762, 729, 697, 657; ^{1}H NMR (300 MHz, $CDCl_3$): δ 1.21 (6H, d, J = 7.0 Hz), 2.12 (3H, s), 2.8–2.9 (1H, m), 5.20 (2H, d, J = 6.1 Hz), 5.39 (2H, d, J = 6.1 Hz), 6.52 (1H, s), 6.76 (1H, s), 7.1–7.2 (4H, m), 7.3–7.5 (7H, m), 7.5–7.6 (4H, m), 7.96 (1H, s); ^{13}C NMR (75 MHz, $CDCl_3$): δ 18.5 (CH_3), 22.3 (CH_3), 22.6 (CH_3), 30.7 (*i*Pr-CH), 65.7 (*N*-CH), 81.2 (η^6-*p*-cymene-CH), 82.9 (η^6-*p*-cymene-CH), 97.5 (η^6-*p*-cymene-C_q), 102.2 (η^6-*p*-cymene-C_q), 119.7 (imidazole-CH), 127.1, 127.7, 128.0, 128.5, 128.8, 128.9, 129.1 (Ar-CH), 132.1 (imidazole-CH), 136.8 (Ar-C_q), 137.9 (Ar-C_q), 140.0 (imidazole-CH), 140.2 (Ar-C_q), 141.7 (Ar-C_q); HRMS for $C_{32}H_{32}N_2ClRu$ [M^+ - Cl] calcd. 581.12920, found 581.12794; Anal. Calc. for $C_{32}H_{32}N_2Cl_2Ru$: C, 62.34; H, 5.23; N, 4.54; found: C, 62.42; H, 5.19; N, 4.51.

4.1.5. Dichlorido(benzene)(CBZ)ruthenium(II) **(1e)**

Climbazole (33 mg, 0.114 mmol) was dissolved in acetone (5 mL) and [Ru(benzene)Cl_2]$_2$ (29 mg, 0.057 mmol) was added. The reaction mixture was stirred at 70 °C for 3 h. *n*-Hexane (50 mL) was added and the formed precipitate was collected, washed with *n*-hexane and dried in vacuum. Yield: 30 mg (0.056 mmol, 49 %); brown solid of mp > 200 °C (dec.); ^{1}H NMR (300 MHz, $CDCl_3$): δ 1.25 (9H, s), 5.6–5.7 (6H, m), 6.55 (1H, s), 6.79 (2H, d, J = 8.4 Hz), 7.1–7.2 (3H, m), 7.42 (1H, s), 8.09 (1H, s); ^{13}C NMR (75 MHz, $CDCl_3$): δ 26.3 (*t*Bu-CH_3), 43.8 (*t*Bu-C_q), 82.9 (*N*-CH), 84.1 (η^6-benzene-CH), 118.1 (imidazole-CH), 118.5 (Ar-CH), 129.7 (C_q), 130.3 (Ar-CH), 132.2 (imidazole-CH), 140.6 (imidazole-CH), 153.5 (C_q), 203.1 (CO); HRMS for $C_{21}H_{23}O_2N_2Cl_2Ru$ [M^+ - Cl] calcd. 507.01746, found 507.01823; Anal. Calc. for $C_{21}H_{23}O_2N_2Cl_3Ru$: C, 46.46; H, 4.27; N, 5.16; found: C, 46.39; H, 4.30; N, 5.11.

4.1.6. Dichlorido(p-cymene)(CBZ)ruthenium(II) **(1f)**

Climbazole (66 mg, 0.228 mmol) was dissolved in CH_2Cl_2 (5 mL) and [Ru(*p*-cymene)Cl_2]$_2$ (70 mg, 0.114 mmol) was added. The reaction mixture was stirred at room temperature for 3 h. *n*-Hexane (50 mL) was added and the formed precipitate was collected, washed with *n*-hexane and dried in vacuum. Yield: 59 mg (0.099 mmol, 43 %); amber solid of mp 109–111 °C (dec.); ν_{max} (ATR)/cm^{-1}: 3113, 3060, 2931, 2875, 1728, 1587, 1448, 1388, 1309, 1276, 1209, 1173, 1092, 1064, 1030, 1006, 946, 866, 827, 763, 657; ^{1}H NMR (300 MHz, $CDCl_3$): δ 1.2–1.3 (15H, m), 2.07 (3H, s), 2.8–2.9 (1H, m), 5.2–5.3 (2H, m), 5.4–5.5 (2H, m), 6.56 (1H, s), 6.83 (2H, d, J = 9.0 Hz), 7.15 (1H, s), 7.19 (2H, d, J = 9.0 Hz), 7.33 (1H, s), 8.17 (1H, s); ^{13}C NMR (75 MHz, $CDCl_3$): δ 18.4 (CH_3), 22.2 (CH_3), 22.3 (CH_3), 26.2 (*t*Bu-CH_3), 30.7 (*i*Pr-CH), 43.9 (*t*Bu-C_q), 81.0, 81.1, 82.3 (*N*-CH), 83.0, 83.2, 97.7 (η^6-*p*-cymene-C_q), 102.4 (η^6-*p*-cymene-C_q), 118.2 (imidazole-CH), 118.5 (Ar-CH), 129.8 (C_q), 130.2 (Ar-CH), 132.5 (imidazole-CH), 140.1 (imidazole-CH), 153.4 (C_q) 203.2 (CO); HRMS for $C_{25}H_{31}N_2O_2Cl_2Ru$ [M^+ - Cl] calcd. 563.08006, found 563.07818; Anal. Calc. for $C_{25}H_{31}N_2O_2Cl_3Ru$: C, 50.13; H, 5.22; N, 4.68; found: C, 50.20; H, 5.27; N, 4.65.

4.2. Leishmania major cell isolation, culture conditions, and assays

L. major promastigotes, isolated from a Saudi patient in February 2016, were maintained at 26 °C in Schneider's Drosophila medium (Invitrogen, USA, containing 10 % heat-inactivated fetal bovine serum/FBS and antibiotics), and weekly transferred. The promastigotes (3×10^6 parasite/mL) were cryopreserved and stored in liquid nitrogen. Stationary-phase promastigotes ($1x10^6$) were injected into hind footpads of female BALB/c mice to maintain virulent *L. major* parasites. *L. major* amastigotes were isolated from the infected animals after 8 weeks, and the isolated amastigotes were transformed to promastigotes again upon cultivation in Schneider's medium supplemented with antibiotics and 10 % FBS at 26 °C. Only amastigote-derived promastigotes, which had undergone less than five in vitro passages, were applied for animal infection. The BALB/c mice (male and female individuals) used for this study were obtained from the Pharmaceutical College of the King Saud University, Kingdom of Saudi Arabia, and kept in suitable pathogen-free facilities in accordance with the instructions and rules of the committee of research ethics, Deanship of Scientific Research, Qassim University, permission number 20–03–20.

L. major promastigotes of the logarithmic-phase were cultured in phenol red-free RPMI 1640 medium containing 10 % FBS, and placed on 96-wells plates (10^6 cells mL^{-1}, 200 µL/well), followed by the addition of test compounds (final concentrations of 50, 25, 12.5, 6.25, 3.13, 1.65, and 0.75 µg mL^{-1}) to the cell cultures. Negative controls were cultures containing only DMSO (1 %), and positive control wells were cultures with decreasing concentrations of the antileishmanial reference drug amphotericin B (50, 25, 12.5, 6.25, 3.13, 1.65, 0.75 µg mL^{-1}). The cultures were incubated at 26 °C for 72 h, followed by the assessment of the number of viable promastigotes by colorimetry (tetrazolium salt colorimetric assay, MTT). The formed formazan dye was dissolved by addition of a detergent solution, and the samples were analysed with an ELISA reader at 570 nm. IC_{50} values were calculated from the observed data of three independent experiments [33].

To evaluate the activity of the test compounds against intramacrophageal amastigotes, peritoneal macrophages were isolated from female BALB/c mice (6–8 weeks of age) by aspiration, followed by adding 5×10^4 cells/well to 96-wells plates containing phenol red-free RPMI 1640 medium with 10 % FBS. Incubation at 37 °C for 4 h in 5 % CO_2 atmosphere to allow cell adhesion was followed by removal of the medium and washing of the cells with phosphate-buffered saline (PBS). A suspension of *L. major* promastigotes (200 µL at a ratio of 10 promastigotes: 1 macrophage in RPMI 1640 medium with 10 % FBS) was added to each well, followed by incubation for 24 h at 37 °C in humidified 5 % CO_2 atmosphere, which allows macrophage infection and differentiation of promastigotes to amastigotes. Thereafter, the infected macrophages were washed thrice with PBS, and treated with fresh phenol red-free RPMI 1640 medium supplemented with the test compounds (50, 25, 12.5, 6.25, 3.13, 1.65, and 0.75 µg mL^{-1}). The treated cells were incubated at 37 °C for 72 h in humidified 5 % CO_2 atmosphere. Cultures containing only DMSO (1 %) were applied as negative controls. Cultures with decreasing concentrations of amphotericin B (50, 25, 12.5, 6.25, 3.13, 1.65, and 0.75 µg mL^{-1}) were used as positive controls. After incubation, the medium was removed and the cells were washed, fixed, and stained with Giemsa stain. The amount of infected macrophages was determined microscopically, and IC_{50} values were calculated from the data obtained from three independent experiments [33,54].

4.3. Toxoplasma gondii cell line, culture conditions, and assay

Vero cells (ATCC® CCL81™, USA) were maintained in complete RPMI 1640 medium (Invitrogen, USA) with heat-inactivated FBS in a humidified 5 % CO_2 atmosphere at 37 °C in 96-well plates (5×10^3 cells/well in 200 µL RPMI 1640 medium). After incubation for one day, the medium was removed and the cells were washed with PBS. Then, RPMI

1640 medium containing 2 % FBS and *T. gondii* tachyzoites (RH strain, a gift from Dr. Saeed El-Ashram, State Key Laboratory for Agro-biotechnology, China Agricultural University, Beijing, China) were added to the Vero cells at a ratio of 5 (parasite): 1 (Vero cells). The tests were carried out according to the following scheme:

Control: RPMI 1640 medium with DMSO (1 %).

Experimental: RPMI 1640 medium + test compounds (from stock solutions in DMSO; final concentrations of 50, 25, 12.5, 6.25, 3.13, 1.65, and 0.75 μg mL^{-1}).

The test samples were incubated at 37 °C and 5 % CO_2 for 72 h, followed by washing the cells with PBS, fixation of cells in 10 % formalin, and cell staining with 1 % toluidine blue. The infection index (number of cells infected from 200 cells tested) of *T. gondii* was determined with an inverted photomicroscope, and the inhibition percentage was calculated by using the following equation:

$$Inhibition(\%) = (I\,control) - (I\,Experimental)/(I\,control) \times 100$$

where, 'I Control' is the infection index of untreated cells, and 'I Experimental' refers to the infection index of cells treated with test compounds. The inhibitory activities of the test compounds against *T. gondii* were expressed as IC_{50} (inhibitory concentration at 50 %) values, which were obtained from three independent experiments [33,55].

4.4. In vitro cytotoxicity assay

Vero or macrophage cells were cultured in RPMI 1640 medium with 10 % FBS and 5 % CO_2 at 37 °C for 24 h in 96-well plates (5×10^3 cells/well/200 μL). Then, the cells were washed with PBS, and treated with test compounds in 10 % FBS medium for 72 h at varying concentrations (50, 25, 12.5, 6.25, 3.13, 1.65, and 0.75 μg mL^{-1}). Cells treated only with medium containing 2 % FBS were used as negative control. After incubation, the supernatant was removed, and 50 μL RPMI 1640 medium with MTT (5 mg mL^{-1}) was added, followed by incubation for 4 h. The supernatant was discarded, and DMSO (150 μL) was added to dissolve the formazan dye. A FLUOstar OPTIMA spectrophotometer was used to analyse the samples colorimetrically ($\lambda = 540$ nm), and the results were expressed as CC_{50} values (cytotoxic concentration, which caused a 50 % reduction in viable cells), which were calculated from three independent experiments [33,56].

4.5. Computational approach

4.5.1. Ligands and protein preparations

The geometries of the complexes **1d** and **1e** were optimized with the Gaussian 16 program in gas phase using rwb97xd functional in conjunction with the 3–21 g basis set without any symmetry constraints [57,58]. Frequency computations were performed to ensure that the optimized structures are minima of the potential energy surface.

The crystal structure of calcium-dependent protein kinase-1 from *T. gondii* (PDB ID: 4JBV), in complex with inhibitor UW1268 (resolution 1.95 Å) was downloaded from the RCSB's Protein Data Bank (https://www.rcsb.org/pdb/) [59].

4.5.2. Molecular docking protocol and validation

Docking simulations were performed on selected targets using Molegro Virtual Docker v.6.0.1 (MVD) software [60]. The MVD package uses an algorithm that maintains macromolecule rigidity and ligand flexibility. The X-ray crystal of the studied target was simplified by eliminating ions, cofactors, water molecules and native ligands from the PDB structure. The molecular docking computational protocol used in the current study has been described in detail in previous studies [61–63].

To validate the efficacy of molecular docking method, the native ligand was re-docked in the studied target, and the RMSD value of the formed complex was between 1 and 2 Å, showing the accuracy and the satisfaction of the docking method [64].

4.5.3. Drug-likeness predictions

The SwissADME server (https://www.swissadme.ch/) was used to determine several physicochemical properties, including TPSA, nROT, MW, LogP, nHA, and nHD [53]. These calculations were performed to assess compliance with Lipinski, Veber, and Egan standards.

CRediT authorship contribution statement

Ibrahim S. Al Nasr: Writing – review & editing, Validation, Resources, Methodology, Investigation, Formal analysis, Data curation, Conceptualization. **Ismail Daoud:** Visualization, Software, Methodology, Formal analysis, Data curation. **Waleed S. Koko:** Writing – review & editing, Resources, Methodology, Funding acquisition, Data curation, Conceptualization. **Tariq A. Khan:** Writing – review & editing, Validation, Resources, Methodology, Investigation, Formal analysis, Data curation. **Rainer Schobert:** Writing – review & editing, Resources, Funding acquisition. **Ridha Ben Said:** Writing – review & editing, Validation, Software, Resources, Methodology, Investigation, Formal analysis, Data curation. **Noureddine Amdouni:** Validation, Software, Resources, Funding acquisition, Data curation. **Seyfeddine Rahali:** Validation, Software, Resources, Funding acquisition. **Ali O. Al-Ghamdi:** Validation, Software, Resources, Funding acquisition. **Bernhard Biersack:** Writing – original draft, Supervision, Project administration, Methodology, Investigation, Formal analysis, Data curation, Conceptualization.

Declaration of competing interest

The authors declare that they have no known competing financial interests or personal relationships that could have appeared to influence the work reported in this paper.

Data availability

Data will be made available on request.

Acknowledgements

We are grateful to the College of Applied Health Sciences at Ar Rass, Qassim University.

Appendix A. Supplementary data

Supplementary data to this article can be found online at https://doi.org/10.1016/j.ica.2024.122005.

References

[1] J.C. Dabrowiak, Metals in Medicine, John Wiley & Sons, Chichester, 2009.
[2] B.S. Sekhon, Metalloid compounds as drugs, Res. Pharm. Sci. 8 (2013) 145–158.
[3] M. Galanski, B.K. Keppler, Tumorhemmende metallverbindungen: Entwicklung, bedeutung und perspektiven, Pharm. Unserer Zeit 35 (2006) 118–123.
[4] G. Sava, R. Gagliardi, A. Bergamo, E. Alessio, G. Mestroni, Treatment of metastases of solid mouse tumours by NAMI-A: Comparison with cisplatin, cyclophosphamide and dacarbazine, Anticancer Res. 19 (1999) 969–972.
[5] C. Scolaro, A. Bergamo, L. Brescacin, R. Delfino, M. Cocchietto, G. Laurenczy, T. J. Geldbach, G. Sava, P.J. Dyson, In vitro and in vivo evaluation of ruthenium(II)-arene PTA complexes, J. Med. Chem. 48 (2005) 4161–4171.
[6] R.E. Morris, R.E. Aird, P. del Socorro Murdoch, H. Chen, J. Cummings, N. D. Hughes, A. Parsons, G. Parkin, D.I. Boyd, P.J.S. Jodrell, Inhibition of cancer cell growth by ruthenium(II) arene complexes, J. Med. Chem. 44 (2001) 3616–3621.
[7] S. Swaminathan, R. Karvembu, Dichloro Ru(II)-p-cymene-1,3,5-triaza-7-phosphaadamantane (RAPTA-C): A case study, ACS Pharmacol. Transl. Sci. 6 (2023) 982–996.
[8] C.A. Vock, W.H. Ang, C. Scolaro, A.D. Phillips, L. Lagopoulos, L. Juillerat-Jeanneret, G. Sava, R. Scopelliti, P.J. Dyson, Development of ruthenium antitumor drugs that overcome multidrug resistance mechanisms, J. Med. Chem 50 (2007) 2166–2175.

[9] L. Oehninger, M. Stefanopoulou, H. Alborzina, J. Schur, S. Ludewig, K. Namikawa, A. Munoz-Castro, R.W. Köster, K. Baumann, S. Wölfl, W.S. Sheldrick, I. Ott, Evaluation of arene Ruthenium(II) N-heterocyclic carbene complexes as organometallics interacting with thiol and selenol containing biomolecules, Dalton Trans. 42 (2013) 1657–1666.

[10] F. Hackenberg, H. Müller-Bunz, R. Smith, W. Streciwilk, X. Zhu, M. Tacke, Novel Ruthenium(II) and gold(I) NHC complexes: Synthesis, characterization, and evaluation of their anticancer properties, Organometallics 32 (2013) 5551–5560.

[11] I.S. Al Nasr, W.S. Koko, T.A. Khan, N. Gürbüz, I. Özdemir, N. Hamdi, Evaluation of Ruthenium(II) N-heterocyclic carbene complexes as enzymatic inhibitory agents with antioxidant, antimicrobial, antiparasitical and antiproliferative activity, Molecules 28 (2023) 1359.

[12] A.-C. Munteanu, V. Uivarosi, Ruthenium complexes in the fight against pathogenic microorganisms, Pharmaceutics 13 (2021) 874.

[13] M. Mdaba, T.M. Golding, G.S. Smith, Recent advances in the biological investigation of organometallic platinum-group (Ir, Ru, Rh, Os, Pd, Pt) complexes as antimalarial agents, Molecules 25 (2020) 5276.

[14] A. Martínez, T. Carreon, E. Iniguez, A. Anzellotti, A. Sánchez, M. Tyan, A. Sattler, L. Herrera, R.A. Maldonado, R.A. Sánchez-Delgado, Searching for new chemotherapies for tropical diseases: ruthenium-clotrimazole complexes display high in vitro activity against *Leishmania major* and *Trypanosoma cruzi* and low toxicity toward normal mammalian cells, J. Med. Chem. 55 (2012) 3867–3877.

[15] E. Iniguez, A. Sánchez, M.A. Vasquez, A. Mártinez, J. Olivas, A. Sattler, R. A. Sánchez-Delgado, R.A. Maldonado, The metal-drug synergy: new ruthenium II complexes of ketoconazole are highly active against *Leishmania major* and *Trypanosoma cruzi* and non-toxic to human or murine normal cells, J. Biol. Inorg. Chem. 18 (2013) 779–790.

[16] M. Navarro, E.J. Cisneros-Fajardo, T. Lehmann, R.A. Sánchez-Delgado, R. Atencio, P. Silva, R. Lira, J.A. Urbina, Toward novel metal-based chemotherapy against tropical diseases. 6. Synthesis and characterization of new copper(II) and gold(I) clotrimazole and ketoconazole complexes and evaluation of their activity against Trypanosoma cruzi, Inorg. Chem. 40 (2001) 6879–6884.

[17] N. Fernández-Pampín, M. Vaquero, T. Gil, G. Espino, D. Fernández, B. García, N. Busto, Distinct mechanism of action for antitumoral neutral cyclometalated Pt (II)-complexes bearing antifungal imidazolyl-based drugs, J. Inorg. Biochem. 226 (2022) 111663.

[18] S. Betanzos-Lara, C. Gómez-Ruiz, L.R. Barrón-Sosa, I. Gracia-Mora, M. Flores-Álamo, N. Barba-Behrens, Cytotoxic copper(II), cobalt(II), zinc(II), and nickel(II) coordination compounds of clotrimazole, J. Inorg. Biochem. 114 (2012) 82–93.

[19] I. Al Nasr, F. Ahmed, F. Pullishery, S. El-Ashram, V.V. Ramaiah, Toxoplasmosis and anti-*Toxoplasma* effects of medicinal plant extracts – a mini-review, Asian Pacif. J. Trop. Med. 9 (2016) 730–734.

[20] http://www.who.int/mediacentre/factsheets/fs375/en/; Accessed November 12, 2020.

[21] K. van Bocxlaer, D. Caridha, C. Black, B. Vesely, S. Leed, R.J. Sciotti, G.-J. Wijnant, V. Yardley, S. Braillard, C.E. Mowbray, J.-R. Ioset, S.L. Croft, Novel benzoxaborole, nitroimidazole and aminopyrazoles with activity against experimental cutaneous leishmaniasis, IJP: Drugs Drug Resist. 11 (2019) 129–138.

[22] I. Bennis, L. Belaid, V. de Brouwere, H. Filali, H. Sahibi, M. Boelart, "The mosquitoes that destroy your face": Social impact of cutaneous leishmaniasis in South-Eastern Morocco, a quality study, PLoS One 12 (2017) e0189906.

[23] M. Kassi, A. Afghan, R. Rehman, P.M. Kasi, Marring leishmaniasis: the stigmatization and the impact of cutaneous leishmaniasis in Pakistan and Afghanistan, PLoS Negl. Trop. Dis. 2 (2008) e259.

[24] D.J. Sheehan, C.A. Hitchcock, C.M. Sibley, Current and emerging azole antifungal agents, Clin. Microbiol. Rev. 12 (1999) 40–79.

[25] M.M. Teixeira, D.T. Carvalho, E. Sousa, E. Pinto, New antifungal agents with azole moieties, Pharmaceuticals 15 (2022) 1427.

[26] G.I. Lepesheva, M.R. Waterman, Sterol 14alpha-demethylase (CYP51) as a therapeutic target for human trypanosomiasis and leishmaniasis, Curr. Top. Med. Chem. 11 (2011) 2060–2071.

[27] G.I. Lepesheva, L. Friggeri, M.R. Waterman, CYP51 as drug targets for fungi and protozoan parasites: Past, present and future, Parasitology 145 (2018) 1820–1836.

[28] J.T. Mesquita, T.A. da Costa-Silva, S.E.T. Borborema, A.G. Tempone, Activity of imidazole compounds on *Leishmania* (L.) infantum chagasi: Reactive oxygen species induced by econazole, Mol. Cell. Biochem. 389 (2014) 293–300.

[29] H. Werner, G. Piekarski, The effect of clotrimazole on the pathogen of toxoplasmosis, *Toxoplasma gondii*, Arzneimittelforschung 26 (1976) 53–55.

[30] W. Wigger-Alberti, K. Kluge, P. Elsner, Clinical effectiveness and tolerance of climbazole containing dandruff shampoo in patients with seborrheic scalp exzema, Praxis 90 (1994) 1346–1349.

[31] A. Briš, J. Jašik, I. Turel, J. Roithová, Anti-cancer organoruthenium(II) complexes and their interactions with cysteine and its analogues. A mass-spectrometric study, Dalton Trans. 48 (2019) 2626–2634.

[32] C. Scolaro, C.G. Hartinger, C.S. Allardyce, B.K. Keppler, P.J. Dyson, Hydrolysis study of the bifunctional antitumor compound RAPTA-C, [Ru(η6-p-cymene)Cl2 (pta)], J. Inorg. Biochem. 101 (2008) 1743–1748.

[33] I.S. Al Nasr, R. Hanachi, R.B. Said, S. Rahali, B. Tangour, S.I. Abdelwahab, A. Farasani, M.M.E. Taha, A. Bidwai, W.S. Koko, T.A. Khan, R. Schobert, B. Biersack, p-Trifluoromethyl- and p-pentafluorothio-substituted curcuminoids of the 2,6-di[(E)-benzylidene)]cycloalkanone type: Syntheses and activities against Leishmania major and Toxoplasma gondii parasites, Bioorg. Chem. 114 (2021) 105099.

[34] D. Berg, E. Regel, H.E. Harenberg, M. Plempel, Bifonazole and clotrimazole. Their mode of action and the possible reason for the fungicidal behaviour of bifonazole, Arzneimittelforschung 34 (1984) 139–146.

[35] E. Iniguez, A. Varela-Ramirez, A. Martínez, C.L. Torres, R.A. Sánchez-Delgado, R. A. Maldonado, Ruthenium-clotrimazole complex has significant efficacy in the murine model of cutaneous leishmaniasis, Acta Trop. 164 (2016) 402–410.

[36] K. Katsuno, J.N. Burrows, K. Duncan, R.H. van Huijsduijnen, T. Kaneko, K. Kita, C. E. Mowbray, D. Schmatz, P. Warner, B.T. Slingsby, Hit and lead criteria in drug discovery for infectious diseases of the developing world, Nat. Rev. Drug Discov. 14 (2015) 751–758.

[37] N.H. Salin, R. Noordin, B.O. Al-Najjar, E.E. Kamarulzaman, M.H. Yunus, I.Z. A. Karim, N.N.M. Nasim, I.I. Zakaria, H.A. Wahab, Identification of potential dual-targets anti-*Toxoplasma gondii* compounds through structure-based virtual screening and in-vitro studies, PLoS One 15 (2020) e0225232.

[38] K. Gajurel, C.A. Gomez, R. Dhakal, H. Vogel, J.G. Montoya, Failure of primary atovaquone prophylaxis for prevention of toxoplasmosis in hematopoietic cell transplant recipients, Transpl. Infect. Dis. 18 (2016) 446–452.

[39] C.J. Canfield, M. Pudney, W.E. Gutteridge, Interactions of atovaquone with other antimalarial drugs against *Plasmodium falciparum* in vitro, Exp. Parasitol. 80 (1995) 373–381.

[40] D.P. Dorairaj, J. Haribabu, M. Dharmasivam, R.E. Malekshah, M.K. Mohamed, C. Echeverria, R. Karvembu, Ru(II)-p-cymene complexes of furoylthiourea ligands for anticancer applications against breast cancer cells, Inorg. Chem. 62 (2023) 11761–11774.

[41] T.A. Khan, I.S. Al Nasr, W.S. Koko, J. Ma, S. Eckert, L. Brehm, R. Ben Said, I. Daoud, R. Hanachi, S. Rahali, W.W.J. van de Sande, K. Ersfeld, R. Schobert, B. Biersack, Evaluation of the antiparasitic and antifungal activities of synthetic piperlongumine-type cinnamide derivatives: Booster effect by halogen substituents, ChemMedChem 18 (2023) e202300132.

[42] M. Hamlaoui, I. Hamlaoui, M. Damous, Y. Belhocine, N. Sbei, F.A.M. Ali, M. A. Alghamdi, S. Talab, S. Rahali, H. Merazig, Synthesis of two novel copper (II) complexes as potential inhibitors of HIV-1 protease enzyme: experimental and theoretical investigations, Crystals 12 (2022) 1066.

[43] E.M. Cardew, C.L.M.J. Verlinde, E. Pohl, The calcium-dependent protein kinase 1 from *Toxoplasma gondii* as target for structure-based drug design, Parasitology 2018 (145) (2018) 210–218.

[44] K.K. Ojo, E.T. Larson, K.R. Keyloun, L.J. Castaneda, A.E. DeRocher, K.K. Inampudi, J.E. Kim, T.L. Arakaki, R.C. Murphy, L. Zhang, A.J. Napuli, D.J. Maly, C.L.M. J. Verlinde, F.S. Buckner, M. Parsons, W.G.J. Hol, E.A. Merritt, W.C. van Voorhis, *Toxoplasma gondii* calcium-dependent protein kinase 1 is a target for selective kinase inhibitors, Nat. Struct. Mol Biol. 17 (2010) 601–607.

[45] W.C. van Voorhis, J.S. Doggett, M. Parsons, M.A. Hulverson, R. Choi, S. Arnold, M. W. Riggs, A. Hemphill, D.K. Howe, R.H. Mealy, A.O.T. Lau, E.A. Merritt, D.J. Maly, E. Fan, K.K. Ojo, Extended-spectrum antiprotozoal bumped kinase inhibitors: A review, Exp. Parasitol. 180 (2017) 71–83.

[46] D. Imhof, N. Anghel, P. Winzer, V. Balmer, J. Ramseier, K. Hänggeli, R. Choi, M. A. Hulverson, G.R. Whitman, S.L.M. Arnold, K.K. Ojo, W.C. van Voorhis, J. S. Doggett, L.M. Ortega-Mora, A. Hemphill, In vitro activity, safety and in vivo efficacy of the novel bumped kinase inhibitor BKI-1748 in non-pregnant and pregnant mice experimentally infected with *Neospora caninum* tachyzoites and *Toxoplasma gondii* oocysts, IJP: Drugs Drug Resist. 2021 (16) (2021) 90–101.

[47] R. Sánchez-Sánchez, D. Imhof, Y.P. Hecker, I. Ferre, M. Re, J. Moreno-Gonzalo, J. Blanco-Murcia, E. Mijías-López, M.A. Hulverson, R. Choi, S.L.M. Arnold, K. K. Ojo, L.K. Barrett, A. Hemphill, W.C. van Voorhis, L.M. Ortega-Mora, An early treatment with BKI-1748 exhibits full protection against abortion and congenital infection in sheep experimentally infected with *Toxoplasma gondii*, J. Infect. Dis. 229 (2024) 558–566.

[48] A. Imberty, K.D. Hardman, J.P. Carver, S. Perez, Molecular modelling of protein-carbohydrate interactions. Docking of Monosaccharides in the Binding Site of Concanavalin a, Glycobiology 1991 (1) (1991) 631–642.

[49] T. Luan, C. Jin, C.-M. Jin, G.-H. Gong, Z.-S. Quan, Synthesis and biological evaluation of ursolic acid derivatives bearing triazole moieties as potential anti-*Toxoplasma gondii* agents, J. Enzyme Inhib. Med. Chem. 34 (2019) 761–772.

[50] J. Singh, M. Kumar, R. Mansuri, G.C. Sahoo, A. Deep, Inhibitor designing, virtual screening, and docking studies for methyltransferase: A potential target against dengue virus, J. Pharm. Bioallied Sci. 8 (2016) 188–194.

[51] R. Hanachi, R.B. Said, H. Allal, S. Rahali, M.A. Alkhalifah, F. Alresheedi, B. Tangour, M. Hochlaf, Structural, QSAR, machine learning and molecular docking studies of 5-thiophen-2-yl pyrazole derivatives as potent and selective cannabinoid-1 receptor antagonists, New J. Chem. 45 (2021) 17796–17807.

[52] R.B. Said, R. Hanachi, S. Rahali, M.A. Alkhalifah, F. Alresheedi, B. Tangour, M. Hochlaf, Evaluation of a new series of pyrazole derivatives as a potent epidermal growth factor receptor inhibitory activity: QSAR modeling using quantum-chemical descriptors, J. Comput. Chem. 42 (2021) 2306–2320.

[53] A. Daina, O. Michielin, V. Zoete, SwissADME: A free web tool to evaluate pharmacokinetics, drug-likeness and medicinal chemistry friendliness of small molecules, Sci. Rep. 7 (2017) 42717.

[54] E. Osorio, G. Arango, N. Jiménez, F. Alzate, G. Ruiz, D. Gutiérrez, M.A. Paco, A. Giménez, S. Robledo, Antiprotozoal and cytotoxic activities in vitro of Colombian annonaceae, J. Ethnopharmacol. 111 (2007) 630–635.

[55] H. Jelali, I. Al Nasr, W. Koko, T. Khan, E. Deniau, M. Sauthier, F. Alresheedi, N. Hamdi, Synthesis, characterization and in vitro bioactivity studies of isoindolin-1-3-phosophonate compounds, J. Heterocycl. Chem. 59 (2022) 493–506.

[56] M. Mohsin, K. Khashan, G. Sulaiman, H.A. Mohammed, K.A. Qureshi, A. Apsatwar, A novel facile synthesis of metal nitride@metal oxide (BN/Gd_2O_3) nanocomposite and their antibacterial and anticancer activities, Sci. Rep. 13 (2023) 22749.

[57] M.J. Frisch, G.W. Trucks, H.B. Schlegel, G.E. Scuseria, M.A. Robb, J.R. Cheeseman, G. Scalmani, V. Barone, G.A. Petersson, H. Nakatsuji, et al., Gaussian16 Rev. B.01; Wallingford, CT, 2016.

[58] J.D. Chai, M. Head-Gordon, Long-range corrected hybrid density functionals with damped atom–atom dispersion corrections, Phys. Chem. Chem. Phys. 10 (2008) 6615–6620.
[59] R.S.R. Vidadala, K.K. Ojo, S.M. Johnson, Z. Zhang, S.E. Leonard, A. Mitra, R. Choi, M.C. Reid, K.R. Keyloun, A.M.W. Fox, M. Kennedy, T. Silver-Brace, J.C.C. Hume, S. Kappe, C.L.M.J. Verlinde, E. Fan, E.A. Merritt, W.C. van Voorhis, D.J. Maly, Development of potent and selective *Plasmodium falciparum* calcium-dependent protein kinase 4 (PfCDPK4) inhibitors that block the transmission of malaria to mosquitoes, Eur. J. Med. Chem. 74 (2014) 562–573.
[60] R. Thomsen, M.H. Christensen, MolDock: A new technique for high-accuracy molecular docking, J. Med. Chem. 49 (2006) 3315–3321.
[61] L. Simon, A. Imane, K.K. Srinivasan, L. Pathak, I. Daoud, In silico drug-designing studies on flavanoids as anticolon cancer agents: pharmacophore mapping, molecular docking, and Monte Carlo method-based QSAR modeling, Interdiscipl. Sci. Comput. Life Sci. 2016 (9) (2016) 445–458.
[62] I. Daoud, S. Bouarab, S. Ghalem, Docking, dynamic simulation and quantum mechanics studies of pyrazinamide derivatives as novel inhibitors of acetylcholinesterase and butyrylcholinesterase, Pharma Chem. 7 (2015) 307–321.
[63] A. Toumi, F.I. Abdella, S. Boudriga, T.Y. Alanazi, A.K. Alshamari, A.A. Alrashdi, A. Dbeibia, K. Hamden, I. Daoud, M. Knorr, J.-L. Kirchhoff, C. Strohmann, Synthesis of tetracyclic spirooxindolepyrrolidine-engrafted hydantoin scaffolds: Crystallographic analysis, molecular docking studies and evaluation of their antimicrobial, anti-inflammatory and analgesic activities, Molecules 28 (2023) 7443.
[64] K.E. Hevener, W. Zhao, D.M. Ball, K. Babaoglu, J. Qi, S.W. White, R.E. Lee, Validation of molecular docking programs for virtual screening against dihydropteroate synthase, J. Chem. Inf. Model. 49 (2009) 444–460.